A Circularly Polarized Antenna Based on the Unidirectional Resonant Modes of a Ferrite Disk

Javad Ghalibafan[1], Behzad Rejaei[2], and Nader Komjani[1]

[1]Department of Electrical Engineering, Iran University of Science and Technology, Tehran 16846, Iran
[2]Department of Electrical Engineering, Sharif University of Technology, Tehran 14588, Iran

We propose a circularly polarized antenna with a wide axial ratio (AR) beamwidth that consists of a normally magnetized ferrite disk mounted on a ground plane. The device uses the resonant modes of the disk, which rotate only in the clockwise or counter-clockwise sense in the frequency range where the effective permeability of ferrite is negative. A semianalytical model is derived for the antenna fed by a single, conventional current probe and is validated numerically by finite element method. For a yttrium iron garnet disk with the radius and height of 5 and 1 mm, respectively, the results show a 3 dB AR beamwidth of 90° with an operation frequency, which can be tuned in the 4–4.5 GHz range by varying the magnetic bias field from 50 to 35 000 A/m. Simulations show that higher AR beamwidths are achievable using finite ground conductors. Compared with previous papers, the fabrication requirements on this structure are not critical, which enhances its potential applicability.

Index Terms— **Circular polarization (CP), ferrite loaded antenna, tunable antenna, wide-angle axial ratio (AR).**

I. Introduction

CIRCULAR polarization (CP) is a common polarization type used in wireless systems for frequency identification, global positioning (GPS), and wireless local area networks, since it can provide greater flexibility in orientation angle between transmitter and receiver, and better mobility and weather penetration than the linearly polarized antennas. For some of these applications, such as GPS, the candidate antenna must have a very broad angular range for CP. In such cases, however, conventional circularly polarized microstrip antennas are inadequate, since their axial ratio (AR) beamwidth is normally narrow, and is restricted around the antenna boresight [1], [2]. Furthermore, the usable, simultaneous impedance, and AR bandwidths cannot be wide enough [3], [4].

The above-mentioned issues have been addressed by a multitude of techniques. In [5], a regular CP antenna on a 3-D square ground has been proposed whose 3 dB AR beamwidth is $\sim$113°; however, the height of the proposed antenna exceeds 0.45 wavelength. In [6], an 85° AR beamwidth has been realized by integrating two bowtie patch antennas and two trapezoidal-shaped dipoles. This structure needs a hybrid or Wilkinson power divider in its feeding network. The use of stacked and multilayer structures [7], [8], flatly folded conducting walls on a pyramidal ground plane [9], and phased arrays [10] are other methods to realize wide beamwidth CP antennas.

In this paper, we present a compact circularly polarized, wide-angle AR antenna that consists of a normally magnetized ferrite disk mounted on a ground plane and covered, on top, by a thin conducting disk. The idea here is to realize CP properties using unidirectional resonant modes rotating only in the clockwise or counter-clockwise sense in a frequency range where ferrite material exhibits negative effective permeability. Compared with previous paper, the fabrication requirements on this structure are not critical, which enhances its potential applicability. Using theoretical results, we show that the proposed antenna easily achieves a 90° AR beamwidth. The structure can be fed by a single, conventional current probe that decreases the cost and complexity of the fabrication process. Moreover, the 3 dB AR and -10 dB return loss bandwidths can be frequency tuned by changing the dc bias magnetic field applied to the ferrite. This feature eliminates the narrow bandwidth problem in [3] and [4].

It is noteworthy that antennas on ferrite substrates have been known to possess useful properties such as frequency tunability [11], low radar cross-sectional scattering [12], and beam scanning [13]. In addition, in several works, antennas printed on magnetized ferrite substrates have been found to radiate CP [14], [15]. However, due to the coupling between two opposite CPs, the AR beamwidths reported were not wide enough.

This paper is organized as follows. Section II outlines the operation principle of the antenna. The complete antenna with its feeding network is described in Section III. In Section IV, the theory of Sections II and III is validated by full-wave simulations and the results are discussed.

II. Operation Principles of the Antenna

Fig. 1(a) shows the proposed antenna, which consists of a disk of ferrite material mounted on a ground plane and covered by a thin circular metal patch. The ferrite disk is magnetized normal to the ground plane by a dc bias magnetic field H_0, which can be provided by a permanent magnet placed underneath the ground plane, where the interference with the antenna is negligible [16].

Because the vertical wall of the disk is open and exposed to free space, no analytic solution of the problem exists. A semianalytical treatment of this problem will be presented in

Manuscript received June 1, 2013; revised July 27, 2013; accepted September 21, 2013. Date of publication September 26, 2013; date of current version March 14, 2014. Corresponding author: J. Ghalibafan (e-mail: jghalibafan@ee.iust.ac.ir).

Color versions of one or more of the figures in this paper are available online at http://ieeexplore.ieee.org.

Digital Object Identifier 10.1109/TMAG.2013.2283655

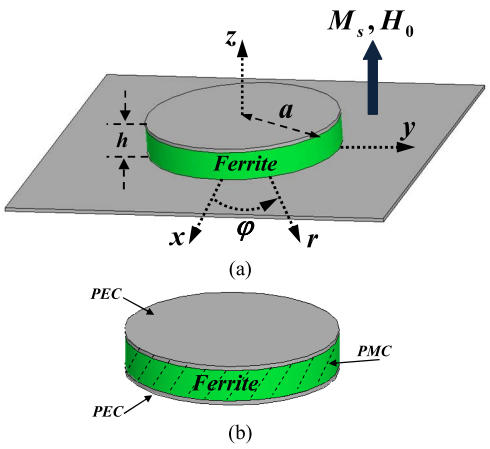

Fig. 1. (a) Geometry of the normally magnetized ferrite disk. (b) Analytical model structure with PMC sidewall approximation.

the following section. However, for the moment, let us follow the classic paper by Bosma [17] and assume the disk wall to be covered by a perfect magnetic conductor (PMC), as shown in Fig. 1(b). This approximation, which is justified if the disk is thin compared with its radius (i.e., $h \ll a$), also allows the neglect of the vertical variation (along z) of the electromagnetic field inside the disk. Finally, to simplify the calculations, the patch and ground plane conductors are taken to be perfect.

From Maxwell equations in cylindrical coordinates, it then follows that the electric field has a z-component only which is governed by the Helmholtz equation [17], [18]:

$$\frac{1}{r}\frac{\partial}{\partial r}\left(r\frac{\partial E_z}{\partial r}\right)+\frac{1}{r^2}\left(\frac{\partial^2 E_z}{\partial \varphi^2}\right)+k_0^2\varepsilon\mu_\perp E_z=0. \tag{1a}$$

The magnetic field is given by $\boldsymbol{H}=H_r\,\hat{\boldsymbol{r}}+H_\varphi\,\hat{\boldsymbol{\varphi}}$ in which

$$H_r=\frac{1}{\omega\mu_0\mu_\perp}\left(\frac{j}{r}\frac{\partial E_z}{\partial \varphi}-\frac{\mu_a}{\mu}\frac{\partial E_z}{\partial r}\right) \tag{1b}$$

$$H_\varphi=\frac{1}{j\omega\mu_0\mu_\perp}\left(-j\frac{\mu_a}{\mu}\frac{1}{r}\frac{\partial E_z}{\partial \varphi}+\frac{\partial E_z}{\partial r}\right). \tag{1c}$$

In these equations, k_0 is the free space wave number, ε is the relative permittivity of ferrite material, μ_0 is the permeability of vacuum, and

$$\mu=1+\frac{\omega_H\omega_M}{\omega_H^2-\omega^2}$$
$$\mu_a=\frac{\omega_M\omega}{\omega_H^2-\omega^2} \tag{1d}$$

are the diagonals, respectively, off-diagonal elements of the permeability tensor of the ferrite where $\omega_H=\gamma H_0$ and $\omega_M=\gamma M_s$, with M_s the saturation magnetization of the ferrite, and γ the gyromagnetic ratio. Moreover

$$\mu_\perp=\mu-\frac{\mu_a^2}{\mu}=\frac{(\omega_H+\omega_M)^2-\omega^2}{\omega_\perp^2-\omega^2} \tag{1e}$$

with

$$\omega_\perp=\sqrt{\omega_H(\omega_H+\omega_M)}. \tag{1f}$$

In (1d) and (1e), magnetic losses may be easily introduced by the replacement $\omega_H=\gamma H_0+j\alpha\omega$, where α is the Gilbert damping constant.

For our purpose, let us now consider the frequency range $\omega_\perp<\omega<\omega_H+\omega_M$, where $\mu_\perp$ becomes negative [see (1e)]. In this case, (1a) is satisfied by the modal solutions

$$E_z^n=A_n\,I_n\,(q_\perp r)\,e^{-jn\varphi} \tag{1g}$$

where n is an integer, A_n is a constant, I_n is the modified Bessel functions of first kind, and

$$q_\perp=k_0\sqrt{-\varepsilon\mu_\perp}. \tag{1h}$$

Substitution of (1g) in (1c) yields

$$H_r^n=\frac{A_n q_\perp}{\omega\mu_0\mu_\perp}\left[\frac{nI_n\,(q_\perp r)}{q_\perp r}-\frac{\mu_a}{\mu}I_n'\,(q_\perp r)\right]e^{-jn\varphi} \tag{1i}$$

$$H_\varphi^n=\frac{A_n q_\perp}{j\omega\mu_0\mu_\perp}\left[-n\frac{\mu_a}{\mu}\frac{I_n\,(q_\perp r)}{q_\perp r}+I_n'\,(q_\perp r)\right]e^{-jn\varphi}. \tag{1j}$$

Note that each mode represents a field rotating in the counter-clockwise ($n>0$) or clockwise ($n<0$) direction. Imposing the PMC boundary condition on the magnetic field in (1j) leads to the following [17]:

$$n\frac{\mu_a}{\mu}=\frac{(q_\perp a)\,I_n'\,(q_\perp a)}{I_n\,(q_\perp a)}. \tag{2}$$

The resonance frequencies of the disk are found by solving the above equation. However, unlike a conventional dielectric disk, the resonance frequencies of the counter-clockwise and clockwise modes are not equal as the left-hand side of (2) depends on the sign of n. In fact, because the right-hand side of (2) is always positive, only clockwise rotating solutions with $n<0$ are possible since $\mu_a/\mu<0$ in the frequency range of interest. The electric field of these resonant modes, given by (1g), drops exponentially toward the disk center. These modes are, in fact, surface waves propagating on the disk circumference, similar to edge-guided modes in a microstrip built on a vertically magnetized ferrite substrate [19].

Especially, since the electromagnetic field is concentrated near the edge of the disk, we could imagine that if the PMC condition on the disk wall is lifted, a portion of the microwave energy contained within the ferrite disk will radiate into free space. Like a microstrip patch [2], the radiation field may be computed from the equivalent magnetic surface current

$$\boldsymbol{M}_n=E_z^n\hat{\boldsymbol{z}}\times\hat{\boldsymbol{r}}=E_z^n\hat{\boldsymbol{\varphi}} \tag{3}$$

on the disk wall, which yields the far-zone electric field [20]

$$\boldsymbol{E}^f(\boldsymbol{R})=\frac{jk_0e^{-jk_0R}}{4\pi R}\hat{\boldsymbol{R}}\times F_n(\hat{\boldsymbol{R}}) \tag{4}$$

where

$$F_n(\hat{\boldsymbol{R}})=\int_{S'}\boldsymbol{M}_n(\boldsymbol{R}')e^{jk_0\hat{\boldsymbol{R}}\cdot\boldsymbol{R}'}\,ds' \tag{5}$$

is the magnetic current form factor. In these equations, the primed coordinates represent the magnetic current source and the unprimed coordinates represent the observation point.

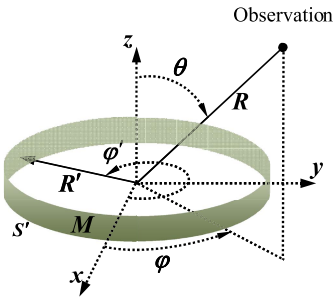

Fig. 2. Equivalent magnetic surface current model for the magnetized ferrite disk structure shown in Fig. 1.

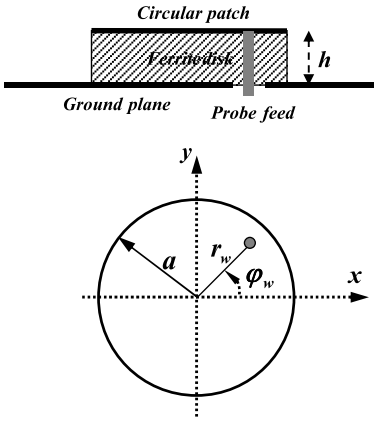

Fig. 3. Cross sectional (top) and top view (bottom) of the ferrite disk with the current probe feed at r_w,φ_w.

After substituting (1g) and (3) into (5), carrying out the integration, and using (4), we obtain the far-zone field

$$\boldsymbol{E}^f(\boldsymbol{R}) = \frac{jk_0 e^{-jk_0 R}}{4\pi R}[F_{n,+}(\hat{\boldsymbol{\varphi}}\cos\theta + j\hat{\boldsymbol{\theta}}) + F_{n,-}(\hat{\boldsymbol{\varphi}}\cos\theta - j\hat{\boldsymbol{\theta}})] \quad (6)$$

where θ is the polar angle in spherical coordinates (Fig. 2), $\hat{\boldsymbol{\theta}}$ is the corresponding unit vector, and

$$F_{n,\pm} = 2\pi ahA_n j^n I_n(q_\perp a)\, e^{\mp j\varphi} \times \sin(k_0 h\cos\theta)\, J_{n\mp1}(k_0 a\sin\theta). \quad (7)$$

If the radius of the ferrite disk is much smaller than the free space wavelength (λ_0), then $k_0 a\sin\theta \ll 1$. Besides, since only negative values of n are allowed, we have

$$\left|\frac{F_{n,+}}{F_{n,-}}\right| = \left|\frac{J_{n-1}(k_0 a\sin\theta)}{J_{n+1}(k_0 a\sin\theta)}\right| \sim \left(\frac{k_0 a\sin\theta}{2}\right)^{2|n|}. \quad (8)$$

The second term inside the bracket in (6) will thus be much larger than the first term so that

$$\boldsymbol{E}^f(R) \sim \frac{k_0 e^{-jk_0 R} F_{n,-}}{4\pi R}\left(\hat{\boldsymbol{\theta}} + j\hat{\boldsymbol{\varphi}}\cos\theta\right). \quad (9)$$

The polarization of this electric field is left-handed elliptical with the AR given by

$$AR = 20\log_{10}\left(\frac{1}{\cos\theta}\right). \quad (10)$$

The resulting 3 dB AR, which is a measure of CP, has a beamwidth of 90° ($-45° < \theta < 45°$). Besides, the AR is independent of the azimuthal angle φ, which is a direct consequence of the absence of the counter-clockwise rotating fields. Therefore, the structure of Fig. 1 can be used as a wide-angle circularly polarized antenna. Note also that the state of polarization can be switched by reversing the direction of the bias magnetic field [15], which now results in counter-clockwise resonating modes and right-handed elliptical polarization. Finally, from (7), it follows that for disks, which are small in comparison with λ_0, the highest far-field amplitude (therefore highest radiated power) for a given amplitude of the surface electric field is obtained for $n = -1$.

III. Antenna Model With Current Probe Feed

Now, we employ the idea presented above to design a wide-angle AR antenna. To excite the $n = -1$ mode, a simple current-probe feed consisting of a thin wire is used, which pierces the ferrite disk and connects to the circular metal patch on top (Fig. 3). In what follows, we compute the impedance of the resulting antenna.

As an approximation, the variation of the probe current in the z-direction is neglected. Next, we analyze the response of the ferrite disk to an infinitely thin electric current line source carrying a constant current i_0 and traversing the disk at the position r_0, φ_0. The current density of the line source is

$$\boldsymbol{J}_i = \hat{\boldsymbol{z}}\frac{i_0}{r_0}\delta(r - r_0)\,\delta(\varphi - \varphi_0). \quad (11)$$

Note that (1a) is still valid for $r < r_0$ and $r > r_0$. Hence, for $r < r_0$, we expand the field in modal solutions [see (1g) and (1j)]

$$E_z^<(r,\varphi) = \sum_{n=-\infty}^{\infty} A_n I_n(q_\perp r)\, e^{-jn\varphi} \quad (12a)$$

$$H_\varphi^<(r,\varphi) = \frac{q_\perp}{j\omega\mu_0\mu_\perp}\sum_{n=-\infty}^{\infty} \times A_n\left[-n\frac{\mu_a}{\mu}\frac{I_n(q_\perp r)}{q_\perp r} + I_n'(q_\perp r)\right]e^{-jn\varphi}. \quad (12b)$$

The radial component of the magnetic field is not given here. Similarly, for $r > r_0$, we may write

$$E_z^>(r,\varphi) = \sum_{n=-\infty}^{\infty}[B_n I_n(q_\perp r) + C_n K_n(q_\perp r)]\, e^{-jn\varphi} \quad (13a)$$

$$H_\varphi^>(r,\varphi) = \frac{q_\perp}{j\omega\mu_0\mu_\perp}\sum_{n=-\infty}^{\infty} B_n\left[-n\frac{\mu_a}{\mu}\frac{I_n(q_\perp r)}{q_\perp r} + I_n'(q_\perp r)\right]e^{-jn\varphi} + \frac{q_\perp}{j\omega\mu_0\mu_\perp}\sum_{n=-\infty}^{\infty} C_n\left[-n\frac{\mu_a}{\mu}\frac{K_n(q_\perp r)}{q_\perp r} + K_n'(q_\perp r)\right]e^{-jn\varphi} \quad (13b)$$

in which modified Bessel functions of the second kind (K_n) are also considered since the origin is excluded.

For the determination of the constants A_n, B_n, and C_n, we match the fields at the position of the line source by demanding

$$E_z^{<}(r_0,\varphi) = E_z^{>}(r_0,\varphi) \tag{14a}$$

$$H_\varphi^{>}(r_0,\varphi) - H_\varphi^{<}(r_0,\varphi) = \frac{i_0}{r_0}\delta. \tag{14b}$$

However, for a full solution of the problem, an extra boundary condition is needed at the disk edge at $r = a$. In general, this is a complicated problem similar to that of radiation from the open end of a waveguide. Mathematically, it is impossible to locally match the tangential components of the electromagnetic field of the disk given by (13a) and (13b) for $r = a$, with the free space field as modes with a z-dependent field distribution or different polarization have been neglected.

In a dielectric waveguide, a strategy to circumvent this problem is outlined in [21]. Here, the distribution of the electric field on the boundary surface is equated to that of the main propagating mode in the waveguide, which is then used to calculate the magnetic field outside the guide (in free space). However, instead of demanding the tangential components of the calculated magnetic field and the waveguide mode to match, only the total complex power crossing the boundary surface is required to be continuous. Following this approach for each mode n, we find that at the boundary of the disk, the azimuthal component of the magnetic field must be given by

$$H_\varphi^{>}(a,\varphi) = -\sum_{n=-\infty}^{\infty} y_n \left[B_n I_n(q_\perp a) + C_n K_n(q_\perp a)\right] e^{-jn\varphi}. \tag{15}$$

The details of the calculation are presented in the Appendix. The complex quantity y_n represents the admittance of the free space region observed at the disk boundary in the nth mode and, for a thin ferrite disk, is given by

$$y_n = \frac{U_n}{\frac{1}{2} - N_n} \tag{16}$$

$$U_n = \omega\varepsilon_0 a \int_0^\infty \frac{\sin^2(k_z h)}{k_z^2 h}\left[J_n'(k_\rho a)\, H_n^{(2)\prime}(k_\rho a) + \frac{k_z^2 n^2}{k_0^2 k_\rho^2 a^2} H_n^{(2)}(k_\rho a) J_n(k_\rho a)\right] dk_z \tag{17}$$

$$N_n = \int_0^\infty \frac{\sin^2(k_z h)}{k_z^2 h}\left[\frac{1}{\pi} + j(k_\rho a) J_n'(k_\rho a) H_n^{(2)}(k_\rho a)\right] dk_z \tag{18}$$

where $H_m^{(2)}$ is the Hankel function of the second kind and

$$k_\rho^2 = k_0^2 - k_z^2. \tag{19}$$

Next, we calculate A_n, B_n, and C_n by substituting (12a)–(13b) in (14a), (14b), and (15), multiplying these equations by $e^{jm\varphi}$, and computing their integral over φ from 0 to 2π. This yields an algebraic system of equations for A_n, B_n, and C_n whose solution is substituted back into (12a) and (13a) to evaluate the electric field inside the disk. This field is in fact the Green's function of the disk (response to a line source) and equals

$$G(\mathbf{r},\mathbf{r}_0) = -\frac{j\omega\mu_0\mu_\perp}{2\pi} K_0(q_\perp|\mathbf{r}-\mathbf{r}_0|) + \frac{j\omega\mu_0\mu_\perp}{2\pi}\sum_{n=-\infty}^{\infty} \chi_n I_n(q_\perp r)\, I_n(q_\perp r_0) \times \exp[-jn(\varphi-\varphi_0)] \tag{20}$$

where $\mathbf{r}$ and $\mathbf{r}_0$ are the 2-D position vector of the observation point, respectively, line source in the horizontal $(x-y)$ plane and

$$\chi_n = \frac{\left(j\omega\mu_0\mu_\perp a y_n - n\frac{\mu_a}{\mu}\right) K_n(q_\perp a) + (q_\perp a) K_n'(q_\perp a)}{\left(j\omega\mu_0\mu_\perp a y_n - n\frac{\mu_a}{\mu}\right) I_n(q_\perp a) + (q_\perp a) I_n'(q_\perp a)}. \tag{21}$$

In the above derivation, we have used the addition theorem for Bessel functions [22]. It is noteworthy that the second term on the right-hand side of (21) drops exponentially toward the center of the ferrite disk. Also, it is noteworthy that the poles of the Green's function, i.e., the zero's of the denominator of χ_n, correspond to the (damped) resonances of the ferrite disk. For $y_n = 0$, which implies perfect magnetic wall condition [see (15)], these resonances become identical to those given by (2). In general, however, the position of the resonance will be shifted compared with the PMC case due to the imaginary part of y_n. Besides, the real part of y_n, which is caused by radiation into free space, will give the resonances a finite width.

With the Green's function computed, the impedance observed by a wire passing vertically through the ferrite disk can be readily calculated if the wire is viewed as an impressed source of current (full treatment of this problem involves the self-consistence calculation of current density on the wire, which is outside the scope of this paper). To simplify the calculation, we consider a wire with circular cross section carrying a total current of I that is distributed uniformly on its surface. The electric field induced by the wire is

$$E_z(\mathbf{r}) = \frac{I}{\pi d}\oint_C G(\boldsymbol{r},\boldsymbol{r}_0)\, dl_0 \tag{22}$$

where d is the diameter of the wire and C is the boundary of its cross section in the horizontal plane. The impedance observed by the wire is then found by evaluating the complex power delivered by the impressed current, which yields

$$Z = -\frac{1}{\pi I d}\oint_C E_z(\boldsymbol{r})\, dl. \tag{23}$$

Next, we substitute (20) and assume the wire to be thin, i.e., $q_\perp d \ll 1$. This allows us to make the approximation

$$K_0(q_\perp|\boldsymbol{r}-\boldsymbol{r}_0|) \sim -\ln(q_\perp|\boldsymbol{r}-\boldsymbol{r}_0|) \tag{24}$$

and to replace both r, φ and r_0, φ_0 by the (cylindrical) coordinates r_w, φ_w of the center of the wire in the summation (see Fig. 3). The final result for impedance is

$$Z = -\frac{j\omega\mu_0\mu_\perp}{2\pi}\left[\ln\left(\frac{q_\perp d}{2}\right) + \sum_{n=-\infty}^{\infty}\chi_n I_n^2(q_\perp r_w)\right]. \tag{25}$$

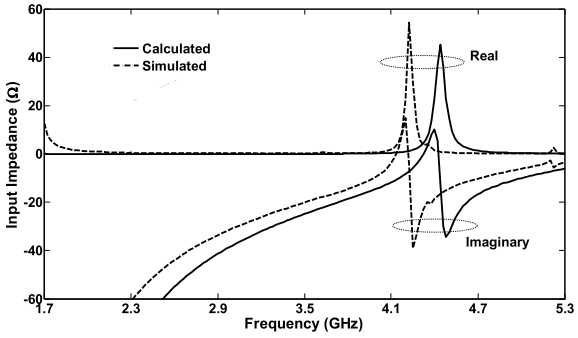

(a)

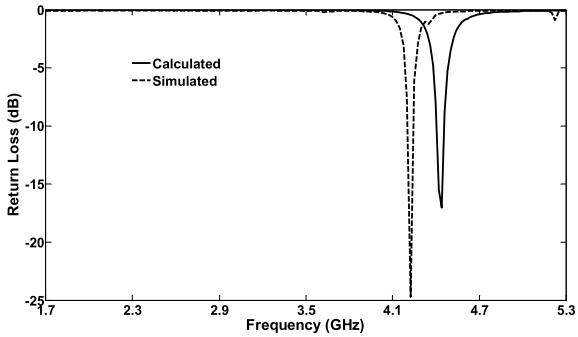

(b)

Fig. 4. Comparison of theoretical and full-wave simulation results for (a) antenna input impedance and (b) return loss. The frequency range is $\omega_\perp < \omega < \omega_H + \omega_M \cdot a = 5$ mm, $r_w = 2.1$ mm, $h = 1$ mm, $H_0 = 15000$ A/m, and the ground dimensions $= 80 \times 80$ mm^2.

Near the resonances of the ferrite disk, χ_n becomes very large, which is directly reflected in Z. For matching purposes, Z may also be tuned by changing the probe position r_w.

IV. Results and Discussion

To verify the theoretical results of the previous sections, the ferrite disk antenna of Fig. 3 is simulated by commercial software HFSS, which uses the finite element method. In all the simulations, yttrium iron garnet (YIG) with a saturation magnetization ($4\ \pi M_s$) of 0.173 T, magnetic line width ($\Delta H = 2\alpha\omega/\gamma$) of 10 Oe, and relative permittivity of 15.3 is used as the ferrite disk material.

Fig. 4 shows the input impedance and return loss of the proposed antenna in the frequency range $\omega_\perp < \omega < \omega_H + \omega_M$, where $\mu_\perp$ becomes negative (antenna parameters are given in the caption). The resonance frequency observed in the simulations is 4.225 GHz, whereas the analytical calculation yields 4.440 GHz. We believe that the main reason for this disparity of ~5% is the neglect of the z-dependent modes of the ferrite disk, which may be excited near the disk boundary.

To validate the exponential behavior of electric fields at this resonance frequency, the full-wave field distribution along the circular patch is shown in Fig. 5, which validates the theoretical results given in (1g).

The AR pattern of the antenna at resonance is shown in Fig. 6 where the analytical AR given in (10) is compared with the simulated AR in planes of $\varphi = 0°$ and $\varphi = 90°$. The results demonstrate a 3 dB AR beamwidth of 90°, which is independent of the azimuthal angle φ. Furthermore, from

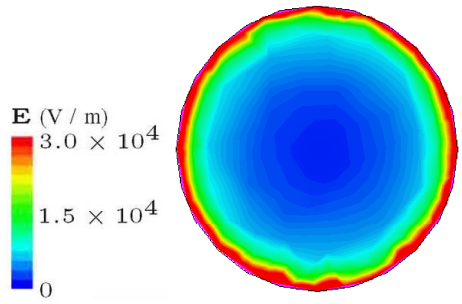

Fig. 5. Electric field distribution computed by HFSS along the circular patch at the resonance frequency. The design parameters are the same as in Fig. 4.

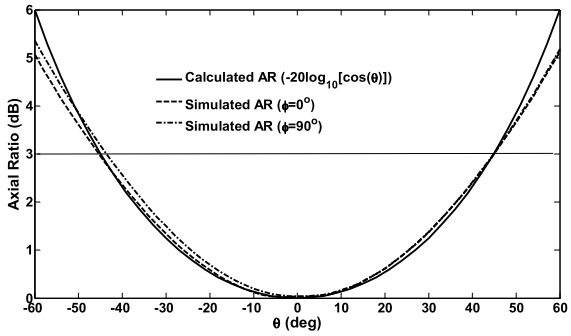

Fig. 6. Comparison of theoretical and full-wave simulation results for AR pattern at the resonance frequency. The design parameters are the same as in Fig. 4.

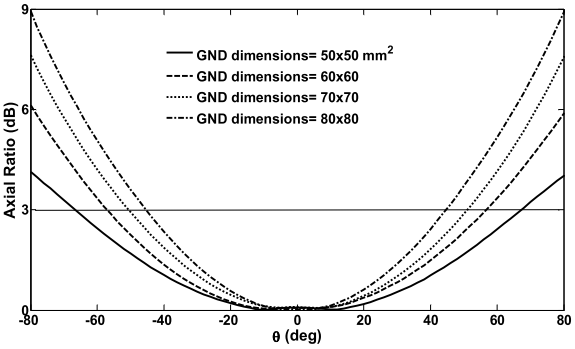

Fig. 7. Full-wave AR pattern at the resonance frequency ($f = 4.225$ GHz) for different ground dimensions. The other design parameters are the same as in Fig. 4.

HFSS simulations, it is observed that using a finite ground and adjusting its dimensions, AR beamwidths much higher that 90° are achievable (Fig. 7). This effect cannot be accounted for by the theory presented in Sections II and III, but we believe that it is caused by additional radiation from the finite ground, which acts as a secondary antenna. Analysis of this effect is too complicated and outside the scope of this paper.

Fig. 8 shows the circularly polarized radiation patterns of the antenna on $x - z$ ($\varphi = 0°$) and $y - z$ ($\varphi = 90°$) planes. The radiation pattern is practically independent of φ, which validates the analytical results in (9). The left-hand circular polarized gain at the resonance frequency is ~7 dB, with the front to back ratio ~13 dB. The back lobe observed is due to the use of a finite ground in the simulations and is decreased by increasing the ground dimensions.

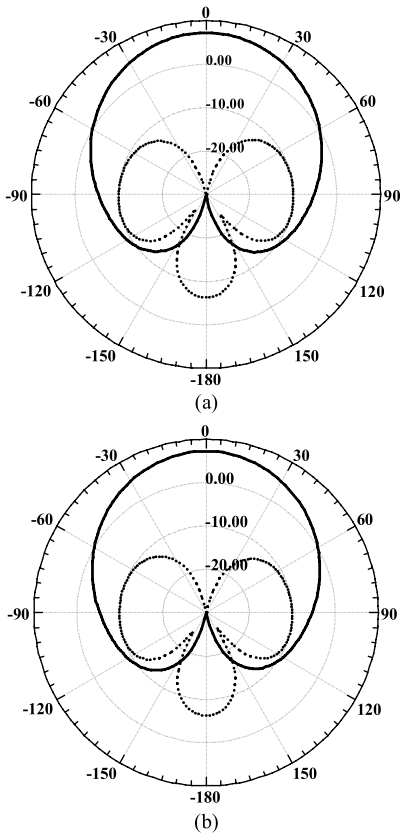

Fig. 8. Circularly polarized radiation patterns at the resonance frequency, the design parameters are the same as in Fig. 4. Dashed line: right-hand circularly polarized pattern. Solid line: left-hand circularly polarized pattern. (a) x-z and (b) y-z plane.

TABLE I
TUNABILITY OF FERRITE DISK ANTENNAS

H_0 (A/m)	Resonance Frequency (GHz)	Return Loss (dB)	Half Power Beamwidth (deg)	3-dB AR Beamwidth (deg)	boresight Gain (dBi)
50	4.025	-12.3	-36 to 36	-48 to 48	7.21
5000	4.100	-15.7	-36 to 36	-46 to 46	7.26
10000	4.150	-17.0	-36 to 36	-46 to 46	7.15
15000	4.225	-24.7	-36 to 36	-45 to 45	7.25
20000	4.300	-12.3	-36 to 36	-45 to 45	7.24
25000	4.350	-14.2	-35 to 35	-44 to 44	7.17
30000	4.425	-12.6	-35 to 35	-44 to 44	7.15
35000	4.500	-9.8	-34 to 34	-44 to 44	7.18

One of the main advantages of the proposed CP antenna is the possibility to tune its operation frequency by changing the magnetic parameters of the ferrite disk. This is achieved by varying the dc bias field H_0 and can compensate for the narrow frequency bandwidth of the antenna (the small impedance frequency bandwidth observed is not a result of the design but due to the high dielectric constant of YIG material used). Table I lists the antenna resonance frequency for various bias fields ranging from 50 to 35 000 A/m. The corresponding resonance frequencies are shifted from 4.025 to 4.500 GHz, which is also evident from the antenna return loss shown in Fig. 9. It is noteworthy that changing H_0 does not

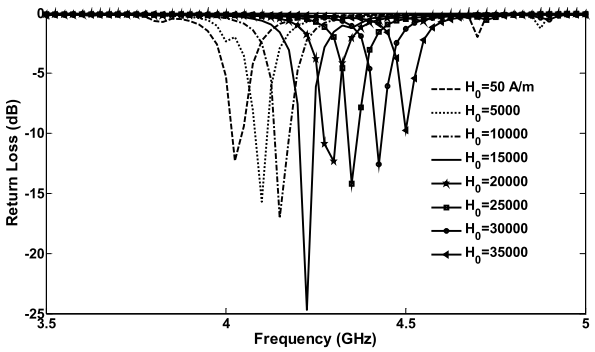

Fig. 9. Full-wave simulated of the return loss against the magnetic bias field. The other design parameters are the same as in Fig. 4.

destroy the antenna radiation parameters, especially the 3 dB AR beamwidth (see Table I). Therefore, the proposed antenna can be used as a frequency tunable CP antenna. Besides, although the third column of Table I lists the upper margin of tunability region to be limited by its impedance matching value, this issue can be resolved by the use of a wideband matching network in addition to the probe.

As a final point, it must be mentioned that the configuration proposed has some similarities with the structures in [14] and [23]. However, the crucial point in this paper is the use of negative permeability, which allows the realization of wide-angle CP properties. This is in contrast with other works where the positive permeability region has been considered. The structure is also different from that of [16], which is based on a leaky wave antenna.

V. CONCLUSION

In this paper, a wide-angle circular polarized antenna is presented, which consists of a normally magnetized ferrite disk on top of a ground plane. For realizing wide-angle CP properties, the ferrite disk is operated in its negative permeability region, where either clockwise or counter-clockwise rotating resonant modes are excited. Using field analysis of the ferrite disk, antenna parameters have been calculated and validated numerically. The results obtained demonstrate a 3 dB AR beamwidth of 90°, which can be potentially increased to $>120°$ by changing the ground dimensions. Moreover, by varying the applied bias magnetic field, the antenna can be frequency tuned without distorting its radiation parameters. Compared with other CP antennas, this structure is compact, is easy to design and fabricate, and does not require a complicated feeding network. As such, it can be a good candidate for realizing wide-angle CP antennas.

APPENDIX

For the derivation of (15)–(18), we take the electric field on the boundary surface (S') of the ferrite disk to be given by (13a) for $r = a$. This field has a z-component only and is z-independent. Next, consider the surface S consisting of S' and parts of the surface of the circular metal patch, which are exposed to free space. With no sources outside the antenna,

application of the extinction theorem [24] to S results in

$$\int_S \nabla \times \bar{\bar{G}}\left(\boldsymbol{R}, \boldsymbol{R}'\right) \cdot \left[\hat{\boldsymbol{n}}' \times \boldsymbol{H}\left(\boldsymbol{R}'\right)\right] dS' = j\omega\varepsilon_0 \int_S \bar{\bar{G}}\left(\boldsymbol{R}, \boldsymbol{R}'\right) \cdot \left[\boldsymbol{E}\left(\boldsymbol{R}'\right) \times \hat{\boldsymbol{n}}'\right] dS' \quad (26)$$

where $\bar{\bar{G}}$ is the dyadic Green function in semi-infinite space bound by the infinite ground plane, $\boldsymbol{n} = \hat{\boldsymbol{r}}$ is the unit normal to S, and $\boldsymbol{R}$ is a point inside the volume enclosed by S.

We neglect the tangential magnetic field on parts of S, which are on the metal patch (tangential electric field automatically vanishes on the patch, which is assumed perfectly conducting). This amounts to the neglect of fringe currents on the patch and allows us to restrict the domain of integration in (26) to S'. Moreover, we disregard the z-component of the magnetic field on S' as it leads to an equivalent electric current ($n \times H_z\, z$) parallel to the ground plane whose effect will be much reduced by its image. From these approximations, and the use of cylindrical coordinates, the φ component of (26) yields

$$-\int_{S'} \frac{\partial G\left(\boldsymbol{R}, \boldsymbol{R}'\right)}{\partial r} H_\varphi\left(\boldsymbol{R}'\right) dS' = j\omega\varepsilon_0 \times \int_{S'} \left[\cos\left(\varphi - \varphi'\right) G\left(\boldsymbol{R}, \boldsymbol{R}'\right) - \frac{1}{k_0^2} \frac{\partial^2 G\left(\boldsymbol{R}, \boldsymbol{R}'\right)}{r r' \partial\varphi \partial\varphi'}\right] E_z\left(\boldsymbol{R}'\right) dS' \quad (27)$$

in which $\boldsymbol{R}_i' = (\boldsymbol{r}', -\boldsymbol{z}')$ is the image of $\boldsymbol{R}' = (\boldsymbol{r}', \boldsymbol{z}')$ with respect to the ground plane at $z = 0$, and

$$G\left(\boldsymbol{R}, \boldsymbol{R}'\right) = \frac{e^{-jk_0|\boldsymbol{R}-\boldsymbol{R}'|}}{4\pi\left|\boldsymbol{R}-\boldsymbol{R}'\right|} + \frac{e^{-jk_0|\boldsymbol{R}-\boldsymbol{R}'_i|}}{4\pi\left|\boldsymbol{R}-\boldsymbol{R}'_i\right|}. \quad (28)$$

Now, consider an individual term of (13a) with the corresponding surface electric field

$$E_z^n = \bar{E}_z^n e^{-jn\varphi} \quad (29)$$

$$\bar{E}_z^n = B_n I_n\left(q_\perp a\right) + C_n K_n\left(q_\perp a\right). \quad (30)$$

We substitute this expression into (27) and use the representation

$$\frac{e^{-jk_0|\boldsymbol{R}-\boldsymbol{R}'|}}{4\pi\left|\boldsymbol{R}-\boldsymbol{R}'\right|} = \frac{1}{8\pi j} \sum_{m=-\infty}^{\infty} e^{-jm(\varphi-\varphi')} \int_{-\infty}^{\infty} J_m\left(k_\rho r\right) H_m^{(2)}\left(k_\rho r'\right) e^{-jk_z(z-z')} dk_z \quad (31)$$

where $r < r'$ and k_ρ is given by (19). After carrying out the integrations, and letting $r \to a$, it follows that on S'

$$H_\varphi\left(\varphi, z\right) = \bar{H}_\varphi^n\left(z\right) e^{-jn\varphi} \quad (32)$$

where H_φ^n satisfies the integral equation

$$\frac{1}{2}\bar{H}_\varphi^n\left(z\right) - \int_0^h F_n\left(z, z'\right) \bar{H}_\varphi^n\left(z'\right) dz' = -\omega\varepsilon_0 a \bar{E}_z^n W_n\left(z\right) \quad (33)$$

where $0 < z < h$ and

$$F_n\left(z, z'\right) = \frac{1}{\pi} \int_0^\infty \cos\left(k_z z\right) \cos\left(k_z z'\right) \left[1 + j\pi\left(k_\rho a\right) J_n'\left(k_\rho a\right) H_n^{(2)}\left(k_\rho a\right)\right] dk_z \quad (34)$$

$$W_n\left(z\right) = \int_0^\infty \frac{\sin\left(k_z h\right) \cos\left(k_z z\right)}{k_z} \left[J'_n\left(k_\rho a\right) H_n^{(2)'}\left(k_\rho a\right) + \frac{k_z^2 n^2}{k_0^2 k_\rho^2 a^2} H_n^{(2)}\left(k_\rho a\right) J_n\left(k_\rho a\right)\right] dk_z. \quad (35)$$

The term in (34) under the brackets will rapidly vanish once $|k_\rho a| > 1$. Thus, only those values of k_z for which $|k_\rho a| < 1$ will contribute to the integral. From (19), it then follows that for a thin ferrite disk, i.e., $h \ll a$, $k_0 h \ll 1$, the arguments of the cosines in (34) are very small as $z, z' < h$. Therefore, F_n is almost constant and may approximated by its average value

$$F_n^{av} = \frac{1}{h^2} \int_0^h \int_0^h F_n\left(z, z'\right) dz dz'. \quad (36)$$

The complex power crossing S' for each mode is

$$P_n = \frac{1}{2} \int_{S'} E_z^n \left(H_\varphi^n\right)^* dS. \quad (37)$$

Since the modal electric field is independent of z, P_n becomes proportional to the average field

$$\frac{1}{h} \int_0^h \bar{H}_\varphi^n\left(z\right) dz = \frac{-\omega\varepsilon_0 a \bar{E}_z^n}{1/2 - h F_n^{av}} \frac{1}{h} \int_0^h W_n\left(z\right) dz \quad (38)$$

where (33) has been used. Because P_n is continuous, the z-independent magnetic field inside the disk will approach the above value for each n as $r \to a$ from within the disk. Substitution of (35) in (38) will then result in (15)–(18).

REFERENCES

[1] C. Wu, L. Han, F. Yang, L. Wang, and P. Yang, "Broad beamwidth circular polarisation antenna: Microstrip-monopole antenna," *Electron. Lett.*, vol. 48, no. 19, pp. 1176–1178, Sep. 2012.

[2] R. Garg, P. Bhartia, I. Bahl, and A. Ittipiboon, *Microstrip Antenna Design Handbook*. Boston, MA, USA: Artech House, 2001.

[3] H. Iwasaki, "A circularly polarized small size microstrip antenna with a cross slot," *IEEE Trans. Antennas Propag.*, vol. 44, no. 10, pp. 1399–1401, Oct. 1996.

[4] J. H. Lee and J. M. Woo, "Design of a L-type aperture coupled circular polarization patch antenna with a single feed," in *Proc. 5th Antennas, Propag. EM Theory Int. Symp.*, Beijing, China, Aug. 2000, pp. 14–17.

[5] C. L. Tang, J. Y. Chiou, and K. L. Wong, "Beamwidth enhancement of a circularly polarized microstrip antenna mounted on a three-dimensional ground structure," *Microw. Opt. Technol. Lett.*, vol. 32, no. 2, pp. 149–153, Jan. 2002.

[6] K. M. Mak and K. M. Luk, "A circularly polarized antenna with wide axial ratio beamwidth," *IEEE Trans. Antennas Propag.*, vol. 57, no. 10, pp. 3309–3312, Oct. 2009.

[7] M. Koubeissi, Y. Abdallah, E. Arnaud, M. Thevenot, T. Monediere, T. Koleck, *et al.*, "Wideband wideangle circular polarization of a multilayer patch antenna," in *Proc. 4th Eur. Conf. Antennas Propag.*, Limoges, France, Apr. 2010, pp. 1–4.

[8] S. I. Latif and L. Shafai, "Hybrid perturbation scheme for wide angle circular polarisation of stacked square-ring microstrip antennas," *Electron. Lett.*, vol. 43, no. 20, pp. 1065–1066, Sep. 2007.

[9] C. W. Su, S. K. Huang, and C. H. Lee, "CP microstrip antenna with wide beamwidth for GPS band application," *Electron. Lett.*, vol. 43, no. 20, pp. 1062–1063, Sep. 2007.

[10] H. D. Cheng, W. Jian, and G. J. Rui, "Design a wide-scan angle phased-array antenna with circular polarization using a new cross dipole," in *Proc. MMWCST Conf.*, Chengdu, China, Apr. 2012, pp. 1–4.

[11] D. M. Pozar and V. Sanchez, "Magnetic tuning of a microstrip antenna on a ferrite substrate," *Electron. Lett.*, vol. 24, no. 12, pp. 729–731, 1988.

[12] V. Losada, R. R. Boix, and Medina, "Evaluation of the radar cross section of circular microstrip patches on anisotropic and chiral substrates," *IEEE Trans. Antennas Propag.*, vol. 49, no. 11, pp. 1603–1605, Nov. 2001.

[13] A. Henderson and J. R. James, "Magnetized microstrip antenna with pattern control," *Electron. Lett.*, vol. 24, no. 1, pp. 45–47, Jan. 1988.

[14] A. A. Mavridis, G. A. Kyriacou, and J. N. Sahalos, "Analysis of circular patch antenna tuned by a ferrite post," *Microw. Opt. Technol. Lett.*, vol. 46, no. 3, pp. 234–236, Aug. 2005.

[15] K. K. Tsang and R. J. Langley, "Design of circular patch antennas on ferrite substrates," *IEE Proc. Microw. Antennas Propag.*, vol. 145, no. 1, pp. 49–55, Feb. 1998.

[16] T. Kodera and C. Caloz, "Low-profile leaky wave electric monopole loop antenna using the $\beta = 0$ regime of a ferrite-loaded open waveguide," *IEEE Trans. Antennas Propag.*, vol. 58, no. 10, pp. 3165–3174, Oct. 2010.

[17] H. Bosma, "On stripline Y-circulation at UHF," *IEEE Trans. Microw. Theory Tech.*, vol. 12, no. 1, pp. 61–72, Jan. 1964.

[18] D. M. Pozar, *Microwave Engineering*, 3rd ed. New York, NY, USA: Wiley, 2004.

[19] M. E. Hines, "Reciprocal and non reciprocal modes of propagation in ferrite stripline and microstrip devices," *IEEE Trans. Microw. Theory Tech.*, vol. 19, no. 5, pp. 442–451, May 1971.

[20] C. A. Balanis, *Advanced Engineering Electromagnetics*. New York, NY, USA: Wiley, 1989, ch. 6.

[21] R. E. Collin, *Antennas and Radiowave Propagation*. New York, NY, USA: McGraw-Hill, 1985, ch. 4.

[22] M. Abramowitz and I. A. Stegun, *Handbook of Mathematical Functions: With Formulas, Graphs, and Mathematical Tables*. New York, NY, USA: Dover, 1970.

[23] J. S. Roy, P. Vaudon, F. Jecko, and B. Jecko, "Magnetized circular ferrite microstrip antenna," in *Proc. ISAP*, Sapparo, Japan, 1992, pp. 765–768.

[24] L. Tsang, J. A. Kong, and K. H. Ding, *Scattering of Electromagnetic Waves, Theories and Applications*. New York, NY, USA: Wiley, 2000.